

Analysis of submicron Cu–Ta–SiO₂ structures by highly charged ion secondary ion mass spectroscopy

T. Schenkel^{a)}

Lawrence Livermore National Laboratory, Livermore, California 94550

K. J. Wu

Charges Evans and Associates, Redwood City, California 94063

H. Li

OnTrak Systems, Incorporated, Milpitas, California 95035

N. Newman, A. V. Barnes, J. W. McDonald, and A. V. Hamza

Lawrence Livermore National Laboratory, Livermore, California 94550

(Received 15 March 1999; accepted 30 June 1999)

We have analyzed wafers with submicron copper lines on Ta/SiO₂/Si by time-of-flight secondary ion mass spectrometry with highly charged projectiles. The goal of the study was to diagnose the effectiveness of different cleaning solutions during brush scrubbing after chemical mechanical polishing. The advantage of projectiles like Xe⁴⁴⁺ lies in the fact that they produce up to three orders of magnitude more secondary ions than singly charge projectiles. Detection of molecular ions (e.g., Cu oxide, Cu hydrocarbon, and alumina ions) enables a detailed assessment of surface conditions on wafers. Analysis of correlations in secondary ion emission from individual impacts gives insight into the chemical structure and homogeneity on a length scale of about 10 nm. © 1999 American Vacuum Society. [S0734-211X(99)04605-3]

I. INTRODUCTION

Continual miniaturization of electronic device dimensions puts increasing demands on the spatial resolution and sensitivity of surface analytical techniques.¹ Time-of-flight secondary ion mass spectrometry (TOF-SIMS) with focused ion beams from liquid metal ion guns can deliver information on the composition and molecular structure with lateral resolutions down to a few hundred nanometers, but the sensitivity and lateral resolution are interdependent. The number of molecular species in the area of a 1 $\mu\text{m} \times 1 \mu\text{m}$ pixel is about 5×10^6 , and the number of secondary ions that can be detected from this area is limited by the ionization probability in the sputtering event and the transmission of the TOF-SIMS instrument. While instrument transmission can be optimized to $\geq 50\%$, ionization probabilities are generally smaller than 10^{-3} and limit detection sensitivities at high lateral resolution.²

We address this limitation by use of very highly charged instead of singly charged ions as projectiles in TOF-SIMS.^{3,4} Recent progress in ion source development at Lawrence Livermore National Laboratory (LLNL) has made beams of slow ($E_{\text{kin}} = 1 \text{ keV} - 1 \text{ MeV}$) Xe⁴⁴⁺ or Au⁶⁹⁺ available for ion–solid interaction studies.⁵ Such highly charged ions deposit tens to hundreds of keV of electronic excitation energy into nanometer size target volumes. The equivalent power densities are on the order of 10^{14} W/cm^2 . Solids react to this intense, ultrafast ($\leq 5 \text{ fs}$) electronic excitation by the emission of large numbers of secondary electrons (a few hundred),⁶ secondary neutrals (up to 1000)^{3,7} and secondary ions. Both secondary ion yields and ionization probabilities,

i.e., the number of secondary ions emitted per unit of sputtered material from oxidized surfaces, increase strongly as a function of projectile charge.³ On average more than one secondary ion can be detected per incident Au⁶⁹⁺ ion from thin silicon dioxide films on silicon substrates.^{3,4} Yields of detected secondary ions are two to three orders of magnitude higher than those for singly charged ion sputtering. The production of large cluster ions is also strongly enhanced.⁸ Detection of two or more secondary ions from the same impact event enables the application of coincidence counting techniques for analysis of correlations in secondary ion emission.^{4,9} The area probed by individual projectiles has an estimated diameter on the order of 10 nm.¹⁰ In this approach, no direct image of impurity distributions is obtained. However, analysis of correlations from many impact events removes the limitation due to the small number of surface species in each impact area. Consequently, information on the chemical composition and homogeneity of target surfaces becomes available on a length scale of about 10 nm, well beyond practical limits for static TOF-SIMS. In a recent publication, we have demonstrated the practicality of coincidence analysis in a study of impurity localization on micron size W/SiO₂ features.⁴ In the present work, we apply highly charged ion SIMS (HCI-SIMS) to characterization of the cleaning processes following chemical mechanical planarization of submicron Cu–Ta–SiO₂ structures.

II. EXPERIMENT

Highly charged ions were extracted from the electron beam ion trap (EBIT) at LLNL.⁵ The EBIT is a compact (few m² footprint), relatively inexpensive source of highly charged ions like Xe⁴⁴⁺ and Au⁶⁹⁺. Currently, beam intensi-

^{a)}Electronic mail: schenkel2@llnl.gov

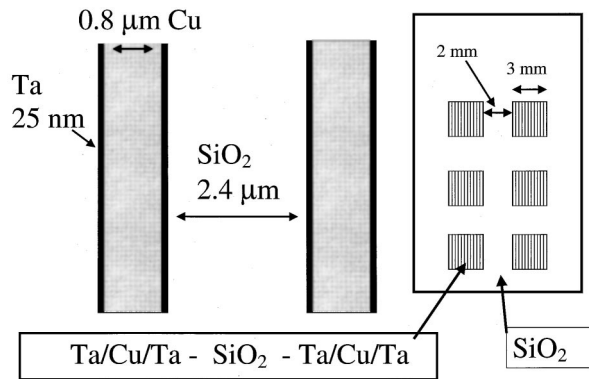
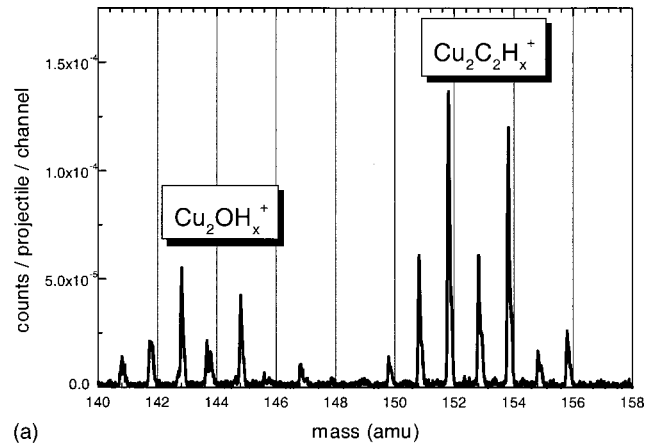


FIG. 1. Schematic of the sample layout with Cu-Ta-SiO₂/Si structures between SiO₂ areas.

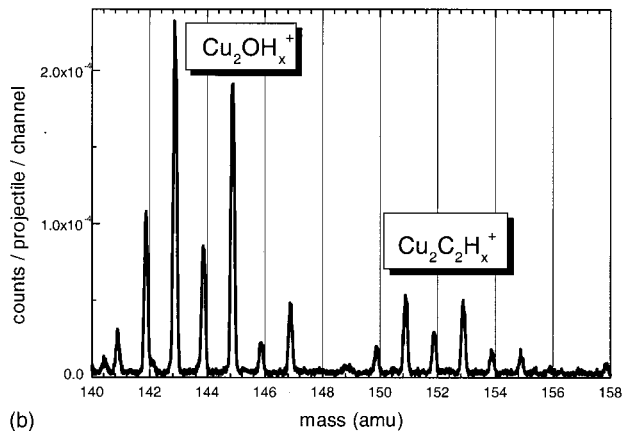
ties up to a few million ions per second can be delivered into a 1 mm² spot. Secondary ions are extracted into a reflectron type secondary ion mass spectrometer. The mass resolution, $m/\Delta m$, was about 2000 at $m = 30 \mu$. In this study we used a beam of Xe⁴⁷⁺ ions with a kinetic energy of 550 keV.

In HCI-SIMS, each time-of-flight cycle is started by the impact of an individual projectile.^{4,11} TOF-SIMS spectra were taken both in histogram mode and in list mode. In the former, TOF cycles from consecutive projectiles are simply summed up to form a spectrum. The accumulation of cycles from the impact of a few million projectiles usually yields sufficient statistics and typical accumulation times are about 10 min. In list mode, time-of-flight cycles (i.e., the start trigger and associated stops from secondary ions) from each projectile are stored separately. Then, conditions on the presence of selected mass peaks are selected when the TOF cycles are summed up. The resulting coincidence spectra show correlations between selected secondary ions or molecular ions that were detected. Each projectile forms secondary ions from a surface area with an estimated size of only a few tens of nanometers. The correlations therefore contain considerable information about local composition.

The targets were silicon wafers with pads of copper lines. The widths of the Cu lines ranged from 0.5 to a few μm. Figure 1 shows a schematic of the sample layout. SiO₂ films with a thickness of 800 nm were deposited on silicon substrates by plasma enhanced chemical vapor deposition (PECVD). The SiO₂ was etched to form trenches after a single mask photolithographic process. After etching, the wafer was covered with a 25 nm thick Ta diffusion barrier layer by physical vapor deposition (PVD). This was followed by PVD of a 50 nm thick Cu seed layer. Then a Cu layer with an excess thickness of about 1 μm was electroplated onto the wafer, filling the trenches and blanketing the whole water surface. The excess Cu and Ta were removed by chemical mechanical polishing (CMP) to expose the SiO₂ and to form the Cu lines and pads. After the polishing, the wafers are cleaned by a double-sided brush scrubber.¹² The two wafer sets analyzed here differed in the cleaning solutions that were used during the brush scrubbing after CMP. For wafer A, the cleaning solution was plain de-ionized wa-



(a)



(b)

FIG. 2. Sections of HCI-SIMS spectra from Cu-Ta-SiO₂ structures. (a) Wafer A (cleaned in de-ionized water), (b) wafer B (cleaned in an acidic solution).

ter. For wafer B a slightly acidic solution of proprietary composition was used. We analyze both areas with Cu lines and areas of blank SiO₂ films between the line pads. The results from different areas on wafers and results from wafers that had undergone similar cleaning processes were consistent.¹³

III. RESULTS AND DISCUSSION

The samples from the two wafer sets differed significantly in the contamination levels of aluminum and copper impurities on the blank SiO₂ areas between structures within a die. Wafer A contained 7×10^{13} aluminum atoms/cm² and copper at the 10^{14} atoms/cm² level. The coverage levels determined by HCI-SIMS agreed well with results from conventional TOF-SIMS and Rutherford backscattering spectroscopy (RBS) (Cu only).¹³ Wafer B showed significantly lower contamination levels (10^{13} Cu/cm² and about 5×10^{11} Al/cm²). The aluminum contamination stems from the use of alumina abrasives in the CMP.^{12,13}

Figures 2(a) and 2(b) show a section of the mass spectrum from the area with copper structures from wafer A (de-ionized water only) and B (acidic solution), respectively. Copper cluster ions are predominantly copper hydrocarbon compounds for wafer A, while the spectrum from wafer B is dominated by copper oxide cluster ions. Copper hydrocarbon

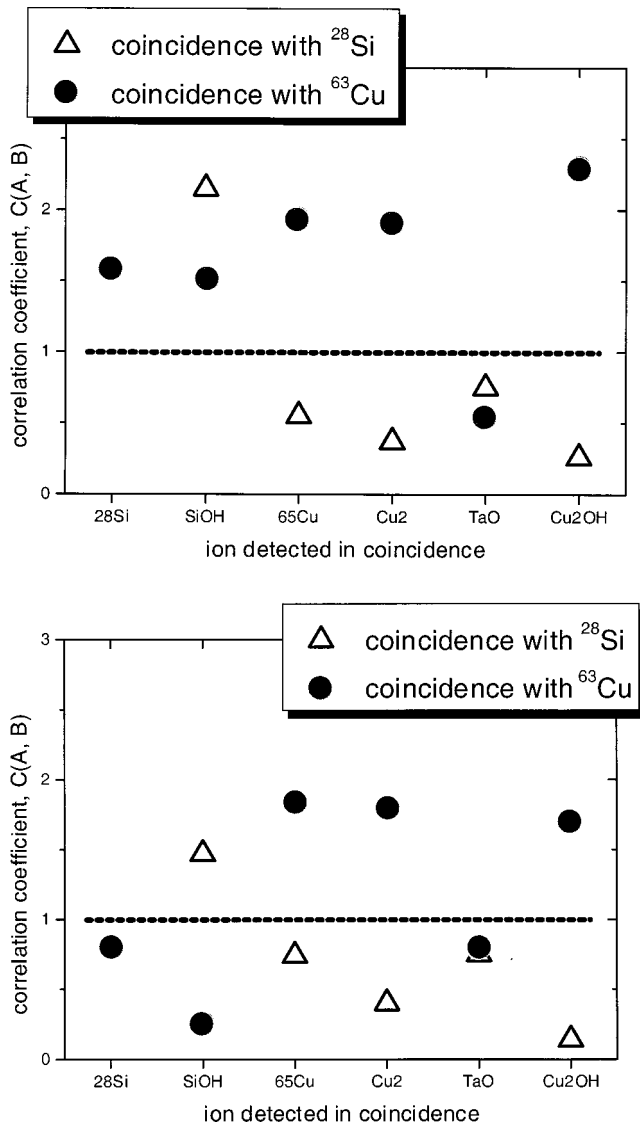


FIG. 3. Correlation coefficients, $C(A, B)$, from coincidence analysis of Cu-Ta-SiO₂ structures. (a) Wafer A, (b) wafer B.

compounds are formed during CMP, where hydrocarbon additives are present in the slurry. These compounds, which are found both on and between structures within a die, passivate the wafer surface and they are not removed by mechanical brush scrubbing with a simple de-ionized water solution. The solution used during brush scrubbing of wafer B was slightly acidic due to a low concentration of HF. Here, copper hydrocarbon residues were removed in the scrubber and the copper could re-oxidize. The copper (oxide) cluster ions were predominantly Cu_n^+ and Cu_nO^+ , with $n=2$ and 3, whereas only very few CuO^+ ions were detected.

We note that these cluster signatures are not observed in conventional TOF-SIMS with singly charged projectiles.¹³

Results from coincidence analysis of a pad of copper lines are shown in Figs. 3(a) and 3(b). The correlation coefficient, $C(A, B)$, gives a measure of the probability of detecting a secondary ion B in coincidence with ion A:^{4,9}

$$C(A, B) = \frac{P(A, B)}{P(A)P(B)}. \quad (1)$$

Here, $P(A)$ and $P(B)$ are the probabilities for the detection of secondary ions A and B in all impact events. $P(A, B)$ is the probability for detection of A and B in the same impact event. For $C(A, B) > 1$, it is more likely that A can be detected when B is also present. For example, the probability of detecting a $^{65}Cu^+$ ion is increased when $^{63}Cu^+$ is also detected in the impact event. $^{65}Cu^+$ and $^{63}Cu^+$ are both emitted when a highly charged ion probes an area on one of the copper lines. On the contrary, $C(A, B) < 1$ indicates an anticorrelation between, e.g., emission of $^{28}Si^+$ and $^{65}Cu^+$ or $^{63}Cu_2^+$. Here, it is very unlikely that both a copper ion and a silicon ion from the same impact event can be detected. This anticorrelation is characteristic for well separated structures of different chemical compositions. The correlation coefficients between wafers A and B differ for $C(Si, Cu)$ and $C(SiOH, Cu)$. Correlation of the copper emission with silicon on wafer A indicates the presence of a blanket, silicon containing residue layer. This blanket contamination is significantly lower on wafer B. The statistical uncertainties in the values of the correlation coefficients are typically smaller than $\pm 20\%$ (not shown).

Detection of TaO^+ ions from the Ta barrier layer is, at the given level of statistical uncertainty, weakly anticorrelated to both silicon and copper ions. This is expected for a well separated, intact barrier layer and also demonstrates that highly charged ions do indeed probe surface features on a length scale of a few tens of nm. Quantification of the area probed by individual projectiles is the subject of ongoing research.¹⁰

A systematic limitation to this correlation analysis lies in the fact that it cannot distinguish the presence of, for example, 100 nm SiO₂ particles on copper lines from well separated copper and SiO₂ areas. This limitation can be addressed by topology analysis using atomic force microscopy.¹³

HCI-SIMS spectra from the SiO₂ areas show high levels of copper and alumina compounds on wafer A [Fig. 4(a)]. Most of these residues have been removed from wafer B [Fig. 4(b)], demonstrating the importance of adding a chemical cleaning component to the mechanical brush scrubbing process.

Coincidence analysis of impurities on SiO₂ areas can address the important question of whether impurities are present as small (≤ 100 nm) particles and/or in a blanket residue deposit [Figs. 5(a) and 5(b)]. Copper particle contamination with coverage levels in the range of 10^{13} atoms/cm² is tolerable for device fabrication, but problems arise when blanket deposits increase the leakage currents between the interconnects.¹³ Copper atoms bound in copper oxide particles do not pose a diffusion hazard, but free copper ions do. The emission probabilities from this homogeneous SiO₂ substrate show an indiscriminately enhanced detection probability in correlations of $^{28}Si^+$ with carbon, aluminum, and copper ions. The probabilities for emission of $^{65}Cu^+$ and Cu_2^+ are increased in the presence of

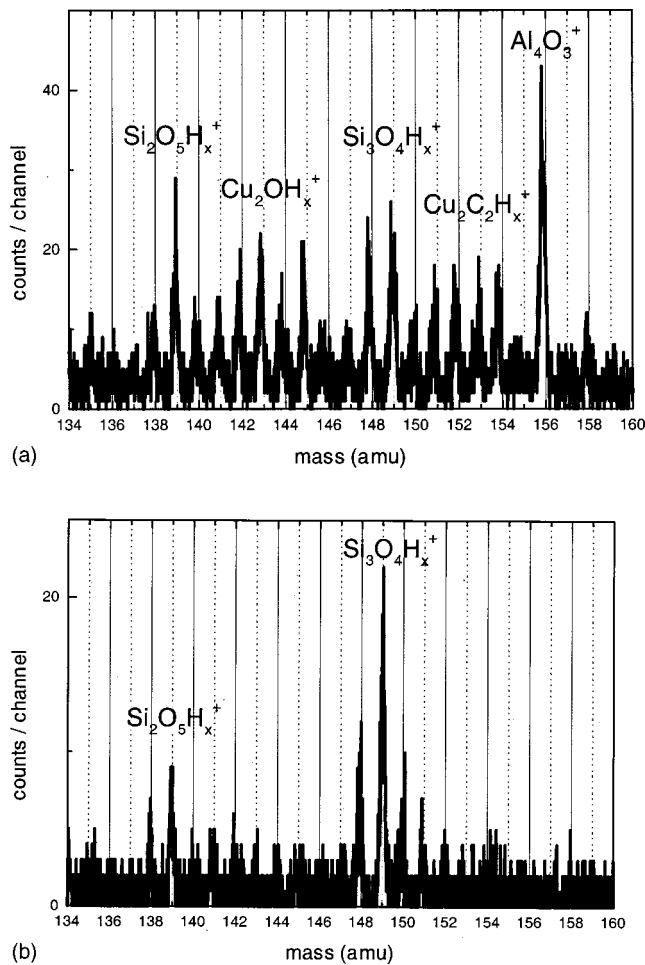
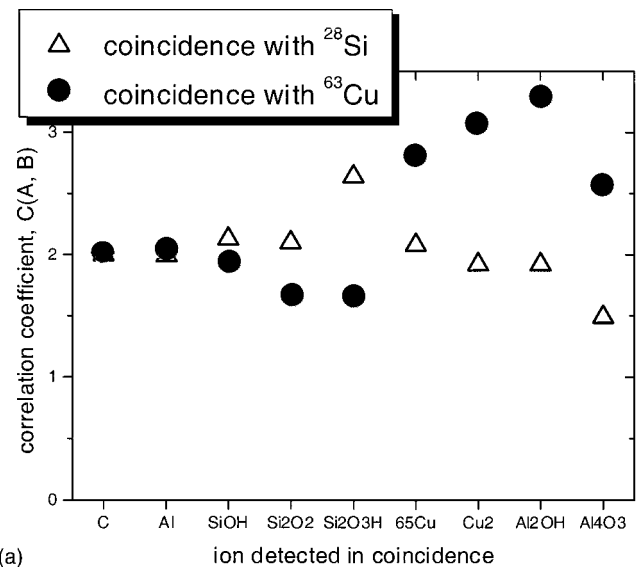


FIG. 4. Sections of HCI-SIMS spectra from a SiO₂ area between Cu-Ta-SiO₂ structures within a die. (a) Wafer A, (b) wafer B.

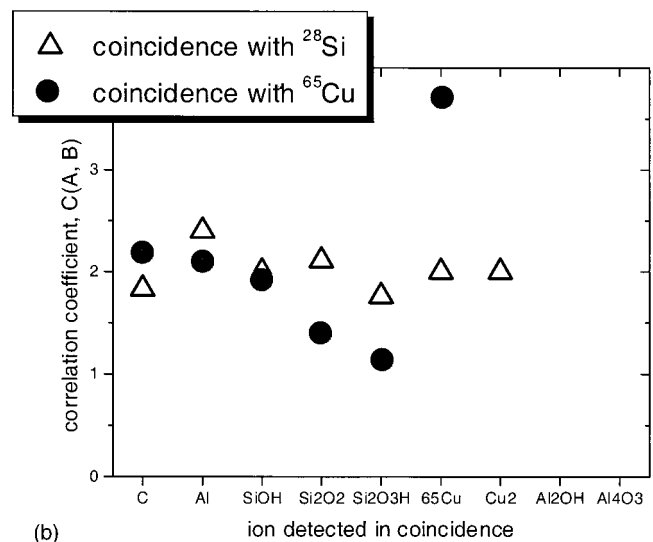
$^{63}\text{Cu}^+$. This enhancement is consistent with the presence of copper particles or “clusters” of copper atoms. The lack of anti-coincidences of copper ions with ions from SiO₂ indicates that these copper clusters are comparable in size or smaller than the area probed by individual projectiles. Anti-correlations are observed between constituents of large (≥ 10 nm), well separated Cu, Ta, and SiO₂ areas (Fig. 3). A blank deposit of copper containing residue would be expected to show no enhanced correlation of $^{63}\text{Cu}^+$ with other copper features. The correlation of $^{63}\text{Cu}^+$ with $^{65}\text{Cu}^+$ on wafers A and B shows that copper atoms are clustered together. Hence the probability of detecting a $^{65}\text{Cu}^+$ ion is enhanced when also detecting a $^{63}\text{Cu}^+$ ion.

The correlation of copper ions with alumina ions (Al_2OH^+ and Al_4O_3^+) could indicate the attachment of copper atoms to small pieces from alumina abrasives.

The brush scrubbing in the acidic solution applied to wafer B etches about 5–10 nm of SiO₂. Consequently, aluminum and aluminum oxide from alumina particles are efficiently removed from wafer B. Copper is still present at the low 10^{13} atoms/cm² level because the solution also etches the copper structures and copper atoms are re-deposited from the



(a)



(b)

FIG. 5. Correlation coefficients from coincidence analysis of a SiO₂ area between Cu-Ta-SiO₂ structures within a die. (a) Wafer A, (b) wafer B.

cleaning solution where they form the above-mentioned small clusters.

A direct comparison of the results from highly charged ion SIMS with results from established imaging techniques, such as atomic force microscopy (AFM) and scanning electron microscopy (SEM) is the subject of current studies.¹⁴

IV. SUMMARY AND CONCLUSIONS

We have shown how HCI-SIMS can be applied to the characterization of cleaning processes within the context of advanced copper metallization. The surface composition and chemical structure of wafers following CMP and different brush scrubbing conditions can be determined. Use of a de-ionized water solution during brush scrubbing leaves high levels of alumina and copper residues on the wafer surface. Use of an acidic cleaning solution adds a vital chemical cleaning component to the mechanical brush scrubbing process, yielding significantly reduced impurity levels.

The results of HCI-SIMS provide important new information on the chemical structure of surface species through efficient detection of cluster ions. Applying coincidence analysis to secondary ion emission, we demonstrate the ability of HCI-SIMS to characterize the chemical structure and homogeneity of surfaces on a length scale of about 10 nm.

ACKNOWLEDGMENT

This work was performed under the auspices of the U.S. Department of Energy by Lawrence Livermore National Laboratory under Contract No. W-7405-ENG-48.

¹*Materials and Bulk Process Roadmap* (Semiconductor Industry Association, San Jose, CA, 1997).

²M. A. Douglas and P. J. Chen, *Surf. Interface Anal.* **26**, 984 (1998); P. K. Chu, B. W. Schueler, F. Reich, and P. M. Lindley, *J. Vac. Sci. Technol. B* **15**, 1908 (1997); A. Schnieders, R. Möllers, M. Terhorst, H.-G. Cramer, E. Niehuis, and A. Benninghoven, *ibid.* **14**, 2712 (1996).

³T. Schenkel, A. V. Barnes, A. V. Hamza, J. C. Banks, B. L. Doyle, and D. H. Schneider, *Phys. Rev. Lett.* **80**, 4325 (1998); T. Schenkel, A. V. Hamza, A. V. Barnes, D. H. Schneider, D. S. Walsh, and B. L. Doyle, *J. Vac. Sci. Technol. A* **16**, 1384 (1998).

⁴A. V. Hamza, T. Schenkel, A. V. Barnes, and D. H. Schneider, *J. Vac. Sci. Technol. A* **17**, 303 (1999).

⁵R. Marrs, P. Beiersdorfer, and D. Schneider, *Phys. Today* **47**, 27 (1994); D. Schneider and M. A. Briere, *Phys. Scr.* **53**, 228 (1996).

⁶J. W. McDonald, D. Schneider, M. W. Clark, and D. Dewitt, *Phys. Rev. Lett.* **68**, 2297 (1992).

⁷T. Schenkel, A. V. Hamza, A. V. Barnes, J. C. Banks, B. L. Doyle, and D. H. Schneider, *Phys. Rev. Lett.* **81**, 2590 (1998).

⁸T. Schenkel, A. V. Hamza, A. V. Barnes, and D. H. Schneider, *Eur. Phys. J. D* **1**, 297 (1998).

⁹E. F. da Silveira, S. B. Duarte, and E. A. Schweikert, *Surf. Sci.* **408**, 28 (1998).

¹⁰T. Schenkel, M. Schneider, M. Hattass, M. W. Newman, A. V. Barnes, A. V. Hamza, D. H. Schneider, R. L. Cicero, and C. E. D. Chidsey, *J. Vac. Sci. Technol. B* **16**, 3298 (1998).

¹¹T. Schenkel, A. V. Barnes, M. A. Briere, A. Hamza, A. Schach von Wittenau, and D. Schneider, *Nucl. Instrum. Methods Phys. Res. B* **125**, 153 (1997); T. Schenkel, M. A. Briere, H. Schmidt-Böcking, K. Bethge, and D. Schneider, *Mater. Sci. Forum* **248–249**, 413 (1997).

¹²D. Hymes, I. Malik, J. Zhang, and R. Emani, *Solid State Technol.* **40**, 209 (1997).

¹³H. Li, D. J. Haymes, J. de Larios, I. A. Mowak, and P. M. Lindley, *Micro March*, 35 (1999), and references therein.

¹⁴I. A. Mowak (private communication).